Simultaneous Ultrasonic Measurement of Thickness and Speed of Sound in Elastic Plates Using Coded Excitation Signals

Daniel A. Kiefer, Michael Fink, *Student Member, IEEE*, and Stefan J. Rupitsch, *Member, IEEE*

Abstract—Layer thickness and the speed of sound are important parameters for nondestructive testing applications. If one of the parameters is known, the other one can be determined by simple time-of-flight (TOF) measurement of ultrasound. However, often these parameters are both unknown. In this contribution, we examine and adapt ultrasonic imaging techniques using coded excitation signals to simultaneously measure the thickness and the speed of sound of homogeneous elastic plates of unknown material. Good axial resolution is required to measure thin samples. We present a new approach for transmission signal conditioning to improve axial resolution. This conditioning consists of enhancing spectral components that are damped by the transducer prior to transmit. Due to the long duration of coded excitation signals, pulse compression techniques are required for TOF measurements. Common pulse compression filters are discussed, and appropriate filtering of the compression waveform is designed to keep the sidelobe level (SLL) acceptably low. An experimental assessment of the presented measurement techniques reveals that the signal conditioning substantially increases the axial resolution. However, a tapered Wiener filter should be used for the best tradeoff between SLL and axial resolution. We used the proposed method to measure different plates of steel, aluminum, and polymethylmethacrylate of various thicknesses, and the results show very good agreement with the reference values, which we obtained with a micrometer screw and by standard TOF measurement, respectively. The relative error for the plate thickness is smaller than 2.2% and that for the speed of sound is smaller than 3%. It is remarkable that plate thickness could be measured down to 60% of the wavelength.

Index Terms—Axial resolution, measurement, plate, pulse compression, simultaneous, speed of sound, thickness, ultrasound.

I. INTRODUCTION

ULTRASONIC nondestructive testing requires the determination of geometric and material parameters, e.g., thickness and the speed of sound. If either one of these parameters is known, the other one can be determined by simple time-of-flight (TOF) measurement of ultrasound. However, these parameters are often both unknown. When measuring a plate, they can be identified simultaneously by exploiting reverberation [1], i.e., multiple reflections that occur at the two layer boundaries producing multiple echoes of the incident acoustic signal. For nondestructive testing applications, the simultaneous determination of properties may be very beneficial, as this allows analysis of samples with unknown and possibly nonuniform parameters, such as biological tissues [2]. In this contribution, we will investigate the use of coded excitation signals and signal conditioning in order to efficiently exploit reverberation for simultaneous measurement of sample thickness and the speed of sound in elastic plates of unknown material.

Determining the sample thickness by means of ultrasound may have some significant advantages. In contrast to most of the established techniques, mechanical contact to the specimen is not required. Only a coupling medium, like water or air, is needed. Among other things, this facilitates measurements with high sampling rates. Furthermore, mechanical waves propagate in basically any medium. Although damping can be rather different, the measurement is highly independent of the specimen material. For example, as already mentioned, material properties, such as the speed of sound, do not necessarily need to be known in advance. In principle, the material density could additionally be identified with the same measurement [3]. Consequently, samples of basically any material can be analyzed as long as they are considerably thinner than half the penetration depth. Moreover, by using reflection mode operation, these measurements can be performed for samples that are only accessible from one side, e.g., coatings.

There are several potential applications for such an instrumentation. For example, the product thickness of a rolling mill could be tested continuously and without contact. Moreover, surface coatings could be characterized during a fabrication process [3], [4]. In the field of medical engineering, it has also been suggested that dentists could measure the thickness of dental enamel for diagnostic purposes [5].

Starting from the late 80s, inverse methods were devised to measure the geometric or acoustic parameters of viscoelastic materials and plates [3], [4], [6]–[10]. These methods operate by adjusting the parameters of a theoretical model until the modeled response matches the measured data. The advantage of inverse methods is that very thin plates can be characterized. Kinra and Iyer [6] reported to have successfully measured the thickness of plates down to 1% of the wavelength. However, as was reported in [3], [4], and [11] and confirmed by own measurements, the convergence region is usually very small. Appropriate initial guesses for the model parameters within the convergence region are, therefore, of utmost importance. Kinra and Iyer [6] tackled this problem by performing a search instead of an optimization algorithm to find the minimal

error between measured data and model; while Bai *et al.* [3] exploited the fact that the number of superimposed echoes increases over time and performed several fitting and subtraction operations. Overall, although very thin plates can be characterized, serious convergence issues make the inverse method approach unattractive, because considerable additional effort is necessary for practical implementation.

Alternative approaches for parameter estimation of a "thick" plate are based on direct TOF measurement of reverberation echoes [2], [11]. A plate is defined to be "thick" if the echoes can be separated in time, i.e., if the ultrasonic measurement system provides a sufficiently high axial resolution. Such an approach will be pursued in this paper by designing a system with best possible axial resolution under the given constraints.

Traditionally, short ultrasonic pulses are used to avoid overlapping of the echoes and fulfill the requirements for axial resolution. However, short pulses result in poor signal-to-noise ratio (SNR) and penetration depth. To solve this issue, coded excitation signals and pulse compression may be utilized instead. Here, we will design an appropriate coded excitation signal and pulse compression filter for plate measurements to provide both high axial resolution and high SNR at the same time. Pre-enhancement of the excitation signal will be exploited to make better use of the available transducer bandwidth compared to traditional short pulse excitation. The performance of different compression filters will be compared in terms of axial resolution and sidelobe level (SLL).

This paper is structured as follows. The principle of operation is outlined in Section II. To understand the system to be measured, the relevant plate models are introduced in Section III. Some implications and basic concepts, e.g., axial resolution, are also discussed at this point. In Section IV, we address the properties that should be satisfied by an appropriate excitation signal and explain the process of signal conditioning for improved axial resolution. Section V discusses pulse compression filters and how windowing or filtering may reduce the SLL. After explaining the laboratory setup and the necessary reference measurement, we present an experimental benchmark of various pulse compression filters compared to conventional pulse-echo operation in Section VI and show some measurement results. Finally, Section VII provides a discussion and an outlook.

II. PRINCIPLE OF OPERATION

Different modes of operation exist for ultrasonic characterization of plates [2]. In this paper, we shall use the transmission mode. The setup is shown in Fig. 1. The homogeneous plate to be measured is positioned between a transmitting and a receiving transducer. The distance L between the transducers and the speed of sound c_w of the surrounding medium are assumed to be known. Then the thickness d of the plate and its speed of sound c can both be calculated after determining the TOFs t_0 and t_1 corresponding to the directly transmitted ultrasound signal $e_{p0}(t)$ and the first reverberation echo $e_{p1}(t)$, respectively. Consequently, the thickness and the speed of sound are determined simultaneously with just one measurement. The index "p" indicates that the signal is an ultrasonic pressure wave.
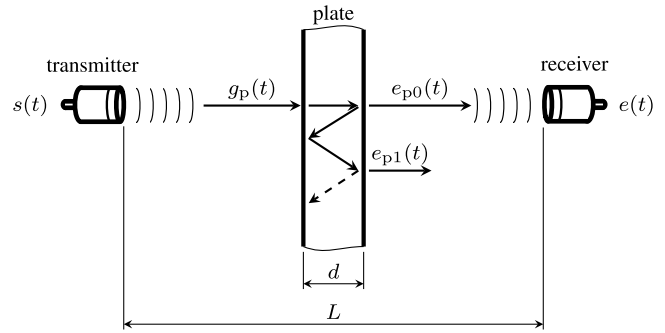
Fig. 1. Principle of operation: propagation of wave fronts is purely in horizontal direction. Vertical components of the ultrasonic rays, visualized as arrows, represent time delays to prior reverberation echoes. Only the relevant rays are shown.

It is easily derived that the sought quantities can be calculated as [1]

$$d = c_w \left(t_w - t_0 + \frac{T}{2} \right) \tag{1}$$

$$c = c_w \left(1 + 2 \frac{t_w - t_0}{T} \right) \tag{2}$$

with $t_w = (L/c_w)$ the TOF without plate and $T = t_1 - t_0$ the delay between two consecutive reverberation echoes. Since c_w and t_w are known from the reference measurement, the aim is to determine the TOFs t_0 and t_1 or equivalently $t_w - t_0$ and T. It is worth noting that the latter two are relative delays and not absolute TOFs. This means that a common time delay, e.g., due to systematic TOF measurement errors, will not affect the measurement result.

III. TRANSMISSION MODEL AND AXIAL RESOLUTION

From a theoretical perspective, the plate can be modeled as a three-layer problem [4], [12]–[14], as shown in Fig. 1. The middle layer represents the homogeneous elastic plate, while the outer layers represent the surrounding fluid medium. An acoustic wave incident on the plate induces a mechanical wave inside it, which again produces an acoustic wave in the surrounding media. We only consider plane waves propagating in normal direction to the layer interfaces. Wave damping is not considered as it is not relevant for the TOFs to be measured. Let us discuss the transmission model of the plate in time and frequency domain as well as the concept of axial resolution in the following sections.

A. Time Domain Transmission Model

At each interface, the incident wave is partially transmitted and partially reflected, causing reverberation in the plate, i.e., an incident wave is not only transmitted through the plate directly, but also after $2n$, $n \in \mathbb{N}$ reflections inside the plate. Hence, a multipath ultrasonic propagation channel is formed. This fact is also sketched for illustrative purposes in Fig. 1.

The directly transmitted signal $e_{p0}(t)$ is received at time t_0. The repeatedly reflected signal $e_{pn}(t)$ shall be called nth-echo and arrives at time

$$t_n = t_0 + nT. \tag{3}$$
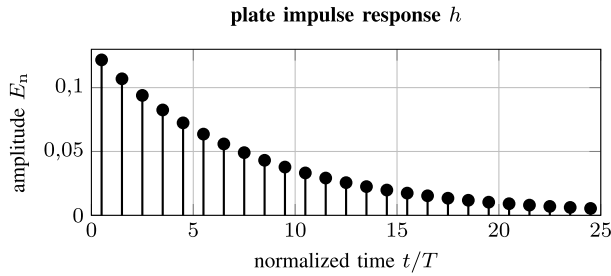
Fig. 2.   Impulse response $h(t)$ of a steel plate in water, where $T = 1.03\ \mu$s.

The time delay

$$T = \frac{2d}{c} = t_{n+1} - t_n \tag{4}$$

corresponds to the time the wave needs to travel back and forth inside the plate. It can, therefore, be treated as a transmission channel characterized by the impulse response

$$h(t) = \sum_{n=0}^{\infty} E_n \delta(t - t_n) \tag{5}$$

where $\delta(t)$ denotes a dirac-pulse and E_n is the amplitude factor given by

$$E_n = q_{wp} q_{pw} r^{2n}. \tag{6}$$

Herein, q_{wp} stands for the transmission coefficient between medium "w" and medium "p," while r is the reflection coefficient. These coefficients depend only on the acoustical impedances Z_w and Z_p of the media "w" and "p," respectively. They are given as [12]

$$q_{wp} = \frac{2Z_p}{Z_p + Z_w} \tag{7}$$

$$q_{pw} = \frac{2Z_w}{Z_p + Z_w} \tag{8}$$

$$r = \frac{Z_p - Z_w}{Z_p + Z_w}. \tag{9}$$

The impulse response contains the information needed to determine the thickness d and the speed of sound c in the plate, namely, the arrival time of the first echo t_0 as well as the time delay T. Fig. 2 illustrates the resulting impulse response of a steel plate in water. The assumed parameters are: acoustical impedance of steel $Z_p = 45.63 \times 10^6$ kg/(m²s), acoustical impedance of water $Z_w = 1.48 \times 10^6$ kg/(m²s), the speed of sound in steel $c = 5850$ m/s, and a plate of thickness $d = 3$ mm [15]. The discussed time domain model is a simple and intuitive description of the plate's transfer behavior. However, some requirements we demand of the excitation signal are best understood by looking at the frequency domain model. We shall, hence, examine this model subsequently.

B. Frequency Domain Transmission Model

The transfer function $H(f)$ of the plate can be obtained as the Fourier transform of (5). The transition time through the plate for the directly transmitted signal is $t_0 = (d/c) = T/2$.
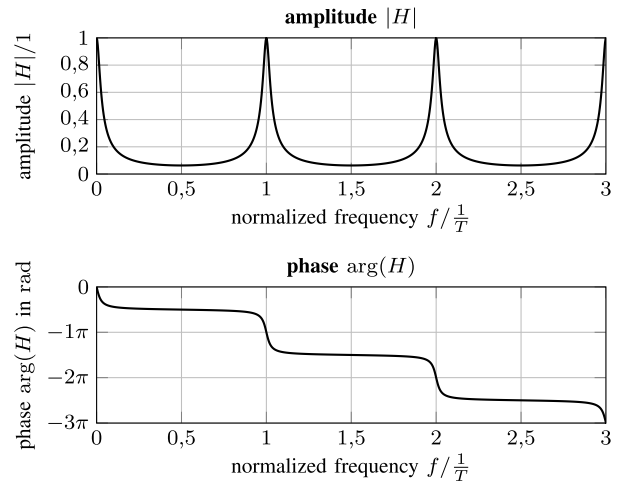
Fig. 3.   Transmission factor $H(f) \bullet\!\!-\!\!\circ h(t)$ of a steel plate in water, where $T = 1.03\ \mu$s.

Denoting the imaginary unit with i and the frequency with f, we obtain the transfer function $H(f)$ as

$$h(t) \circ\!\!-\!\!\bullet H(f) = q_{wp} q_{pw} e^{-i2\pi f \frac{d}{c}} \sum_{n=0}^{\infty} (r^2 e^{-i2\pi f T})^n. \tag{10}$$

Because $|r^2| < 1$ is always satisfied, the geometric series converges and $H(f)$ becomes [16]

$$H(f) = q_{wp} q_{pw} e^{-i2\pi f \frac{d}{c}} \frac{1}{1 - r^2 e^{-i2\pi f T}}$$
$$= \frac{q_{wp} q_{pw}}{e^{i2\pi f \frac{d}{c}} - r^2 e^{-i2\pi f \frac{d}{c}}}. \tag{11}$$

This transfer function is called the frequency dependent transmission factor for the three-layer problem. It can also be deduced from purely harmonic considerations with equivalent result [12].

As can be seen from (11), the transfer function $H(f)$ is periodic, as expected due to the discrete impulse response. The magnitude and phase spectra for the transfer function of a steel plate in water are plotted in Fig. 3. Thereby, the same parameters as for the impulse response of Fig. 2 were assumed.

The periodic peaks in the amplitude spectrum are characteristic for a pulse train. It is interesting to note that the Fourier transform of the infinite pulse train $Ш(t)$ is [17]

$$Ш(t) = \sum_{n=-\infty}^{\infty} \delta(t - nT) \tag{12}$$

$$Ш(f) = \frac{1}{|T|} \sum_{n=-\infty}^{\infty} \delta\left(f - \frac{n}{T}\right). \tag{13}$$

Therefore, a pulse train spaced by T in time domain is again a pulse train spaced by $f_0 = 1/T$ in frequency domain, and we could equivalently use f_0 instead of T to determine d as well as c. When the pulses of the impulse response get closer, the amplitude peaks of the transfer function spread out. Because the actual impulse response of the plate is a

damped sequence of pulses approaching zero, the peaks of the frequency domain transfer function are not Dirac pulses, but rather peaks with nonvanishing width as can be seen in Fig. 3.

The central aim is to determine the delay T. This is solely part of the transfer behavior of the plate. In particular, it does not depend on the excitation signal. Our goal is, therefore, to characterize, at least partly, the transfer behavior. Let us first have a look on some implications so far and some general requirements.

C. Axial Resolution and Measurement Limits

Due to the bandpass behavior of the measurement system, the pulses of the measured impulse response will have a given nonvanishing width. Two pulses can only be identified separately if their time separation is greater than the so-called axial resolution $T_{\min}$. If they are closer, they will melt together into one pulse. Consequently, the smallest detectable delay corresponds to the system's axial resolution.

The magnitude of the signal's envelope is used to determine TOF. Often, the *half-pulsewidth* Δt hereof is taken as a measure for the axial resolution because $\Delta t \approx T_{\min}$, where the exact relation depends on the envelope shape. Unless otherwise required, we shall from now on use the concept of axial resolution and half-pulsewidth interchangeably.

Since thinner plates lead to a smaller time delay T, the lower measurement limit for the plate thickness d is given by the axial resolution of the system and additionally depends on the speed of sound c. By rewriting (4), we find the lower measurement limit $d_{\min}$ for the thickness

$$d_{\min} = \frac{1}{2}c\,\Delta t. \tag{14}$$

Improving the axial resolution is, therefore, equivalent to reducing the lower measurement limit of the system regarding thickness when the speed of sound is constant. On the other hand, it is also equivalent to increasing the upper measurement limit for the speed of sound when the plate thickness is constant.

The goal is to correctly characterize plates as thin as possible with a given fixed available systems bandwidth. This means that the axial resolution has to be improved by choosing an appropriate excitation signal and postprocessing. Although the relevant information is contained exclusively in the plate's impulse response, the axial resolution as well as the achievable SNR does depend on the excitation signal and signal processing used. In the following sections, we will examine the relevant available options.

IV. EXCITATION SIGNAL

The relevant signals in the considered system are shown in the block diagram of Fig. 4. The excitation signal $s(t)$ is the waveform that drives the emitting ultrasonic transducer. Since the system is linear, the transfer blocks of the system components commute. To simplify the subsequent analysis, we combine the emitting and receiving transducer behavior into the two-sided impulse response $h_T(t)$. When excited with $s(t)$, they produce the interrogation signal $g(t) = s(t) * h_T(t)$,
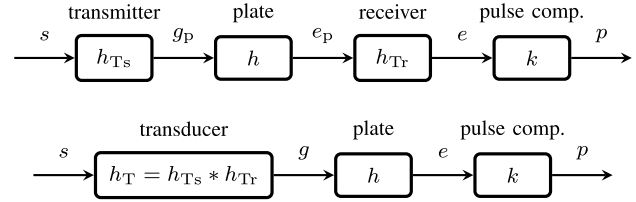
Fig. 4. Two structural diagrams of the measurement system and the arising signals: the upper representation reflects the actual physical setup and the lower one is equivalent and will be used instead throughout this paper. Time dependence of the signals is omitted in favor of conciseness.

where "$*$" denotes temporal convolution. If a plate is placed between the transducers, the system outputs the receiving signal $e(t)$ given by

$$e(t) = s(t) * h_T(t) * h(t) = g(t) * h(t) \tag{15}$$

$$E(f) = S(f)H_T(f)H(f) = G(f)H(f) \tag{16}$$

where lower- and upper-case letters represent Fourier transform pairs.

We can observe from (16) that the excitation signal and the transducer behavior need to be appropriate in order to transfer the desired information of the plate behavior to the received signal $E(f)$. The resulting requirements for the interrogation signal $g(t) = s(t) * h_T(t)$ are presented in the following section.

A. Requirements for the Interrogation Signal

1) Bandwidth: At least one entire period of the plate, transfer function $H(f)$ should be contained in the received signal $E(f)$ to avoid loss of information. The periodicity of $H(f)$ is $1/T$. Hence, the bandwidth B_g of the interrogation signal $G(f) \circ\!\!-\!\!\bullet g(t)$ should be greater than $1/T$. Considering that $T_{\min} \approx \Delta t$ holds, a relationship between axial resolution and signal bandwidth is easily found because

$$B_g \overset{!}{\geq} \frac{1}{T} \Rightarrow T_{\min} = \frac{1}{B_g} \approx \Delta t. \tag{17}$$

It is well known from ultrasonic imaging and radar that axial resolution is inversely proportional to the interrogation signal bandwidth [18]–[20], i.e., a high bandwidth is required to achieve a good axial resolution. This bandwidth is mainly restricted by the employed ultrasonic transducer. We propose a methodology whereby the excitation signal makes best possible use of the available transducer bandwidth, as will be discussed in detail in Section IV-D.

2) Energy: In general, a high SNR is necessary to minimize the detection error of a signal. In ultrasonic imaging and nondestructive testing, a high SNR value also increases the penetration depth into the target [19]. In nondestructive testing, it makes air-coupled testing feasible [21].

To obtain a high SNR, a high-energy interrogation signal should be chosen. Traditionally, this is done by increasing the amplitude of the excitation signal, which has technical limits, though. Furthermore, a sufficiently low mechanical index is required in medical ultrasound.

Signal energy can also be increased by a longer signal duration D and a higher bandwidth B. In classical Fourier theory, the concepts of duration and bandwidth are incompatible since they cannot both be bounded at the same time [22], i.e., a signal with finite duration has an infinite spectrum and vice versa. However, the definition and use of the Gabor duration $\bar{D}$ and Gabor bandwidth $\bar{B}$ [23] results in a meaningful *time-bandwidth product*, which can be used for practical statements about the signal quality. For example, when using a correlation filter for signal detection, the SNR is proportional to the time-bandwidth product $\bar{D}\bar{B}$ [18], [19], [24]. Therefore, SNR can be gained by increasing the time-bandwidth product without the need for higher signal amplitudes.

Due to the uncertainty relationship of signal processing, the time-bandwidth product has a lower limit [23], [25]. Amplitude modulated signals have the lowest time-bandwidth product [19], [24] and among such signals a Gaussian pulse has the lowest one [25]. To achieve a high time-bandwidth product, frequency or phase modulation is necessary. These signals are also called *coded excitation signals* since due to their long duration, a decoding process, commonly referred to as pulse compression, is necessary in order to measure TOF.

B. Chirp Signals

Linear frequency modulated (LFM) signals are also called linear chirp signals. They exhibit good properties as coded excitation signals for ultrasonic imaging [19]. Chirp signals are easy to design with respect to duration and bandwidth, provide good SNR, and with an appropriate pulse compression technique, they also yield a high axial resolution. In this contribution, amplitude modulated linear up-chirp signals will be used for thickness and the speed of sound measurement in plates.

In complex notation, a linear chirp signal has the form

$$\underline{s}_{\text{chirp}}(t) = e^{2\pi i \left(f_c t + \frac{F}{2} t^2 \right)} \quad \text{for} \quad -\frac{D}{2} \leq t \leq \frac{D}{2} \tag{18}$$

with the center frequency f_c, the so-called *chirp rate* $F = B/D$ and the signal duration D, respectively. The chirp excitation signal is the real part of $\underline{s}_{\text{chirp}}$, that is

$$s_{\text{chirp}}(t) = \Re\{\underline{s}_{\text{chirp}}(t)\}. \tag{19}$$

Fig. 5 depicts such a chirp waveform on the left side. The right side shows the corresponding instantaneous frequency f_i. Note that in classical Fourier theory, the concept of instantaneous frequency does not exist. A very good treatment of the topic is given by Cohen [22]. However, for a chirp signal, it makes sense to define the instantaneous frequency as the time-derivative of the exponent in (18) divided by $2\pi i$. Being aware of the fact that the instantaneous frequency of a linear chirp increases linearly with time is helpful for pulse compression filter design in Section V.

C. Wiener Filter

The Wiener deconvolution filter is useful for both signal conditioning and pulse compression. We shall, therefore, introduce it in this section by examining the plate behavior.
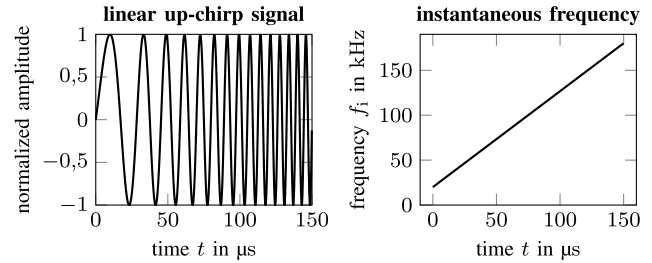
Fig. 5. Up-chirp signal with a center frequency of $f_c = 100$ kHz, bandwidth $B = 160$ kHz (160%), and duration $D = 150$ μs (left) and the corresponding instantaneous frequency f_i (right).

The received signal after transmission through the plate is given by

$$e(t) = g(t) * h(t) \tag{20}$$

where the interrogation signal $g(t)$ and the received signal $e(t)$ after transmission through the plate are both known. In order to reconstruct the plate behavior $h(t)$, we might carry out a deconvolution of the form

$$h(t) = e(t) * g^{-1}(t) \tag{21}$$

$$H(f) = \frac{E(f)}{G(f)} \tag{22}$$

where $g^{-1}(t)$ denotes the inverse of $g(t)$ with respect to convolution. However, this deconvolution by means of the inverse filter $1/G(f)$ is unstable due to the bandpass characteristic of $g(t)$, and it can, thus, not be applied in the presence of noise. The measured received signal $\epsilon(t)$, which is given by

$$\epsilon(t) = g(t) * h(t) + n(t) \circ\!\!-\!\!\bullet \varepsilon(f) \tag{23}$$

is usually corrupted by noise $n(t)$. In this case, an approximate reconstruction $\eta(t) \circ\!\!-\!\!\bullet \varepsilon(f) K_w(f)$ can be performed with the Wiener deconvolution filter $K_w(f)$, which provides a best estimate $\eta(t) \approx h(t)$ in a mean square error sense with best possible noise suppression. Assuming that the noise $n(t)$ is uncorrelated to the signal $h(t)$, the Wiener filter is given by [26] and [27]

$$K_w(f) := \frac{G^*(f)}{G^*(f)G(f) + \Phi_{nn}(f)/\Phi_{hh}(f)} \tag{24}$$

where the noise-to-signal ratio $\Phi_{nn}(f)/\Phi_{hh}(f)$ is given as the ratio of the spectral power densities of the noise $n(t)$ and the unknown target $h(t)$. The difficulty arising when implementing the Wiener filter is that this ratio has to be known, or at least an estimate hereof.

D. Conditioning the Excitation Signal for Improved Axial Resolution

A Dirac pulse has a flat amplitude spectrum. Such an excitation signal makes use of the available bandwidth as provided by the ultrasonic transducer. If the axial resolution of the system is of concern, it might be desirable to make better use of the transducer bandwidth by designing the excitation signal appropriately. Hereinafter, the underlying design process shall be called *signal conditioning*. Previous effort
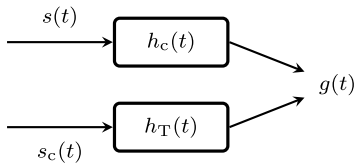
Fig. 6. Convolution equivalence for signal conditioning as proposed in [29].

in this area includes the work of Raman and Rao [28] and Oelze [29], [30].

The main idea of signal conditioning is to compensate for the frequency-dependent damping of the transducer by enhancing the affected spectral components prior to transmission. Consequently, the transducer produces an interrogation signal with a higher bandwidth compared to excitation with a signal having a flat amplitude spectrum and, therefore, the axial resolution will be improved. When performing signal conditioning, SNR is traded for axial resolution. We point out that this conditioning could be applied to any broadband excitation signal including conventional short pulses. However, coded excitation will provide better SNR compared to a short pulse.

1) Conditioning Filter: As proposed by Oelze [29], [30], we shall use the concept of convolution equivalence for signal conditioning (see Fig. 6). The impulse response $h_c(t)$ of a hypothetic transducer with desired properties is designed and shall be called the "conditioned transducer." Mainly, it should provide the desired bandwidth. When excited with the signal $s(t)$, it produces the interrogation signal $g(t)$. The question arising is, what the conditioned excitation signal $s_c(t)$ should be so that the real transducer $h_T(t)$ produces the same interrogation signal. Mathematically, this demands convolution equivalence in the form

$$s_c(t) * h_T(t) \stackrel{!}{=} s(t) * h_c(t) = g(t). \qquad (25)$$

In frequency domain, one can easily solve for the conditioned excitation signal spectrum $S_c(f)$, which yields

$$S_c(f) = S(f) \frac{H_c(f)}{H_T(f)} =: S(f) \Psi(f) \qquad (26)$$

where $\Psi(f)$ denotes the conditioning filter.

However, $H_T(f)$ is a bandpass signal and, therefore, the inverse is not bounded. To achieve a stable deconvolution, a Wiener filter as in (24) can be applied instead to obtain a best estimate of $S_c(f)$. Assuming that in this case the noise-to-signal ratio is of the form $\Phi_{nn}(f)/\Phi_{s_c s_c}(f) = \beta|H_T(f)|^{-2}$, we are able to perform the conditioning with

$$\Psi_w(f) := \frac{H_c(f)H_T^*(f)}{|H_T(f)|^2 + \beta|H_T(f)|^{-2}} \qquad (27)$$

where the parameter $\beta \in \mathbb{R}_+$ is used to estimate the level of noise spectral energy density.

The above conditioning filter $\Psi_w(f)$ tries to accommodate for the phase difference in the two transducers H_c and H_T. As pulse compression is very sensible to phase mismatch [19], this is not a desired behavior because it might degrade the code quality. It might also introduce an undesired time shift

between $s(t)$ and $s_c(t)$. Furthermore, by leaving the phase spectrum unchanged, we are able to transmit the conditioned signal but design the compression filter based on the noncon-ditioned signal. We will see that this might have some relevant advantages. As already mentioned, the main idea is to boost spectral components that are not transmitted efficiently by the transducer. From this point of view, it is evident that applying the conditioning to the magnitude spectrum only should be sufficient. For these reasons, we propose to perform signal conditioning by

$$S_c(f) := S(f)|\Psi_w(f)| = S(f) \frac{|H_c(f)H_T^*(f)|}{|H_T(f)|^2 + \beta|H_T(f)|^{-2}}. \qquad (28)$$

The conditioned excitation signal $s_c(t)$ in time domain results from inverse Fourier transform hereof.

2) Designing the Conditioned Transducer: In order to perform the conditioning as in (28), we first need to design a "conditioned transducer" $h_c(t)$. Oelze [29] applies window functions to the actual transducer impulse response $h_T(t)$ to obtain the conditioned transducer impulse response $h_c(t)$. We present a new approach that gives more control over this design process. The impulse response of a piezoelectric ultrasonic transducer $h_T(t)$ is approximately a Gaussian pulse. It is, therefore, well suited as a model for the conditioned transducer impulse response $h_c(t)$. The advantage is that it can be stated in an explicit analytical form as

$$h_c(t) = e^{\frac{-t^2}{2\sigma^2}} \cos(2\pi f_c t) \qquad (29)$$

with the carrier frequency f_c and a parameter σ defining the time-width of the signal envelope. f_c corresponds to the center frequency of the transducer, while σ determines the transducers bandwidth. According to the modulation theorem, the spectrum of $h_c(t)$ equals the spectrum of its envelope shifted in frequency by f_c. It is, therefore, sufficient to inspect the envelope spectrum in order to assess the signal bandwidth. Performing a Fourier transform of the Gaussian envelope, we obtain [25]

$$e^{\frac{-t^2}{2\sigma^2}} \circ\!\!-\!\!\bullet \sqrt{2\pi}\,\sigma e^{-2(\pi f \sigma)^2}. \qquad (30)$$

By equating the right-hand side of (30) to half of the maximum, i.e., $\sqrt{2\pi}\,\sigma/2$, we find the band limits $f_{\max}$ and $f_{\min}$ and, hence, the −6-dB bandwidth

$$B = f_{\max} - f_{\min} = \frac{\sqrt{2\ln 2}}{\pi\sigma}. \qquad (31)$$

Therefore, it is straightforward to design the conditioned transducer as desired. In particular, the bandwidth B can be chosen freely by setting

$$\sigma = \frac{\sqrt{2\ln 2}}{\pi B}. \qquad (32)$$

E. Selected Excitation Signal

Any coded excitation signal could be used for the proposed measurement method. Measurements for this paper were performed using a conditioned chirp. The conditioned transducer
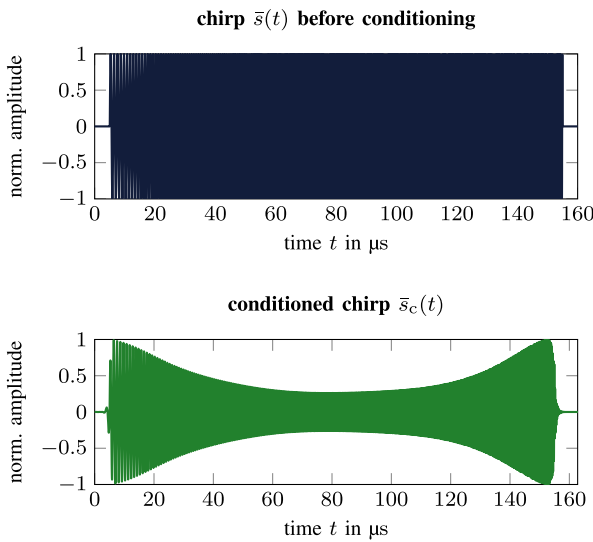
Fig. 7.　Chirp before conditioning (top) and conditioned chirp for improved axial resolution (bottom).

Fig. 8.　Energy density spectra of two interrogation signals $\bar{g}$ and $\bar{g}_c$ obtained by convolution of the excitation signals $\bar{s}$ and $\bar{s}_c$ (see Fig. 7) with the impulse response h_T of the transducer. Each signal is normalized to its maximum magnitude.

Fig. 9.　Received signal $\bar{e}(t)$ for a 3-mm-thick steel plate and $\bar{s}_c(t)$ as excitation signal. Note that echoes arrive at $T \ll D$, resulting in interference.

impulse response $h_c(t)$ was chosen to be a Gaussian pulse matching the transducer's center frequency of 2.29 MHz. Its bandwidth was set to $B_{h_c} = 2.52$ MHz (110%). Conditioning is performed on a linear chirp of duration $D = 150$ μs with center frequency matching the transducer. The chirp's bandwidth was chosen to be $B = 1.14\ B_{h_c} = 2.87$ MHz, which is the optimum bandwidth with respect to SLL (see Section V) for the conditioned transducer [31]. Consequently, the time-bandwidth product is approximately $\bar{D}\bar{B} \approx 430$. This chirp will be referred to as unconditioned excitation signal $\bar{s}(t)$ and is shown at the top panel of Fig. 7. It was conditioned according to (28) and the resulting conditioned excitation signal $\bar{s}_c(t)$ is plotted at the bottom panel of Fig. 7. The conditioning filter noise parameter was chosen empirically as $\beta = 500$. As expected, the frequency components above and below the center frequency have been boosted in the conditioned signal.

These two excitation signals were convolved with the recorded impulse response $h_T(t)$ of the real transducers to obtain the corresponding interrogation signals $\bar{g}(t)$ and $\bar{g}_c(t)$. Their energy density spectra are plotted in Fig. 8. It can clearly be observed that the conditioned interrogation signal exhibits a considerably higher bandwidth than the unconditioned one. Therefore, we expect an improved axial resolution for the conditioned signal.

After transmitting the conditioned chirp $\bar{s}_c(t)$ through a 3-mm-thick steel plate, we receive the signal $\bar{e}(t)$ plotted in Fig. 9. Its envelope magnitude is also shown. Since the echo delay is much smaller than the signal duration, the echoes overlap strongly. Interference results in a characteristic beating, which could be exploited to determine T. However, the quadratic phase of the chirps results in a very complex interference pattern. To identify the echo delay T on the basis of the received signal, we shall instead perform adequate signal processing first, which is subject to the next section.
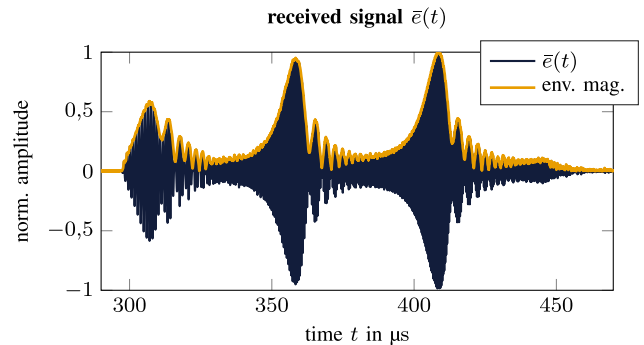
V. Pulse Compression and SLL Reduction

Due to their long duration, the use of coded excitation signals requires pulse compression techniques in order to enable TOF measurements. By means of a decoding process, the energy of the excitation signal is compressed into a short pulse, thereby increasing SNR and restoring axial resolution [24].

After compression of the received signal $e(t)$ with the pulse compression filter $k(t)$, we obtain the pulse compression waveform $p(t)$ (see Fig. 4). The TOFs can be read out of the *compression output* $\iota(t)$, which is the magnitude of the compression waveform envelope. We use the Hilbert transform $\mathcal{H}\{\}$ to compute the envelope, thus obtaining the compression output as

$$\iota(t) = |\mathcal{H}\{p(t)\}| = |\mathcal{H}\{e(t) * k(t)\}|. \quad (33)$$

The resulting compression output does not only consist of a main peak at the signal arrival time, which is called the mainlobe, but also of undesired sidelobes. These sidelobes represent artifacts resulting from the pulse compression process. The ratio of the highest sidelobe height to mainlobe height in decibels is called the sidelobe-level (SLL). Ideally, it should be as low as possible. The half-pulsewidth Δt of the mainlobe is a measure for the axial resolution and it should be as narrow as possible.

Pulse compression techniques are well established in radar and more recently also in ultrasonic imaging [18], [19]. Various filters for pulse compression have been suggested. The matched filter is the most common. Mismatched filters are designed to reduce the SLL. The Wiener filter is an optimal filter for ultrasonic imaging in the sense that it achieves best possible SNR and axial resolution in the presence of noise as well as speckle [19]. However, at least an estimate for the SNR in the received signal is needed. When linear chirp signals are used, the fractional Fourier transform (FrFT) [5], [32]–[34] may also be applied for pulse compression. Nevertheless, it does not provide a higher axial resolution than the prior mentioned filters. Like for the matched filter, pulse compression with FrFT results in a sinc-waveform and, therefore, also provides a resolution of about the inverse bandwidth [33]. In addition, the FrFT exhibits the same problems with inherently high SLL and it is not a standard algorithm. Its main advantage lies in the possibility to separate echoes overlapping in time [32], which is not necessary for our application. The FrFT will, therefore, not be considered further.

Usually, the main idea of pulse compression is to set the phase spectrum of a frequency or phase modulated signal to zero. For a bandpass signal with rectangular amplitude spectrum, this produces a harmonic time domain signal with sinc-shape envelope. As mentioned above, the sinc-functions mainlobe width is approximately equal to the inverse signal bandwidth, i.e., a broadband signal produces a narrow pulse in time domain. Thus, similar axial resolution as for pulse-echo operation is achieved. Since the sidelobes of the sinc-function are high, namely, -13.2 dB below the mainlobe, windowing is often applied to reduce them. SLL reduction will be discussed in detail after the relevant pulse compression techniques have been presented.

A. Pulse Compression

Commonly, pulse compression is performed with a matched filter that is also called correlation filter or conjugate filter. Knowing the transmitted signal waveform in advance, we can use the matched filter to detect the signal. The matched filter in time and frequency domain reads as [17]

$$k_m(t) := s^*(-t) \tag{34}$$

$$K_m(f) = S^*(f) = |S(f)|e^{-i \arg S(f)}. \tag{35}$$

In addition, a sufficient time delay needs to be added in order to obtain a causal filter. Since we record all signals prior to signal processing, we choose the noncausal representation as given in (34) and (35).

The presented measurement system is a transmission system with the task of detecting the arrival time of the transmitted signal and its echoes. Let us assume that the transmission system does not distort the transmitted signal in any way, i.e., the transfer function of the transmission system fulfills $H_S(f) = 1$. Accordingly, the transmitted and received signals are the same. Because the filter is complex conjugate to the transmitted signal, it sets the phase spectrum of the received signal to zero. But the transfer function of the transmission

system in our case is $H_S(f) = H_T(f)H(f)$. Then, if the filter is applied to the received signal $E(f) = H_S(f)S(f)$, only the phase characteristics of the transmission system will remain in the phase spectrum because

$$K_m(f)E(f) = |S|^2|H_S|e^{i(-\arg S + \arg H_S + \arg S)} \tag{36}$$

$$= |S|^2|H_S|e^{i \arg H_S} \tag{37}$$

where the argument f has been omitted for conciseness. If the transmission system introduces a time delay, which corresponds to a linear phase term in frequency domain, it will, therefore, be recovered by the filter since it is contained in $\arg H_S$. This is a desired behavior for TOF measurements. Any nonlinear phase distortions introduced by the transmission system will also remain, potentially producing undesirable effects. Such distortions are mostly produced by the transducer and not the plate. Hence, to mitigate these effects, one can match the receiving filter to the interrogation signal $g(t)$ instead of $s(t)$, such that $K_m(f) = G^*(f)$. In doing so, the filter will also remove phase distortions introduced by the transducer. However, in order to design this filter, the interrogation signal $g(t)$ needs to be known in advance.

A more intuitive approach to pulse compression is deconvolution. The measuring system aims to reconstruct the impulse response $h(t)$ of the plate. For this purpose, we can carry out a deconvolution with a Wiener filter as given in (24). Because we do not possess any *a priori* knowledge of Φ_{hh}, the noise-to-signal ratio shall be assumed constant in frequency, i.e., $\Phi_{nn}(f)/\Phi_{hh}(f) := 1/\text{SNR}_0$. The resulting Wiener filter for pulse compression reads as

$$K_w(f) := \frac{G^*(f)}{G^*(f)G(f) + 1/\text{SNR}_0}. \tag{38}$$

This filter behaves similar to the inverse filter on spectral components with good SNR, but like the correlation filter where signal power density is low. As a consequence, the signal band of the reconstructed signal widens, similar to the use of the inverse filter. A well-designed Wiener filter, thus, improves the axial resolution over conventional matched filtering. It is interesting to note that, similar to the matched filter, the complex conjugate appears in the numerator of (38).

B. SLL Reduction

The mentioned compression filters are linear filters, which means that the superposition principle holds. If several echoes are received, the corresponding pulse compression waveforms superimpose. In the compression output, their mainlobes appear at time instances of echo arrival. If the sidelobes are too high, they might get mistaken for a mainlobe of an actual echo. For this reason, a sufficiently low SLL is critical. However, the requirements are lower than for ultrasonic imaging, where sidelobes degrade the image quality. Our experience showed that for plate measurements, an SLL ≤ -30 dB should be targeted.

There are two main causes for the appearance of sidelobes in the compression waveform $p(t)$ and the corresponding compression output $\iota(t)$ [35]. The first one are sharp band edges in the compression waveform amplitude spectrum $|P(f)|$.

The second one are ripples in this amplitude spectrum $|P(f)|$, which manifest as so-called *paired echoes* in the corresponding time domain signal. It should be noted that these paired echoes produce undesired sidelobes and are not linked to reverberation echoes originating in the plate. For signals with high time-bandwidth product ($\bar{D}\bar{B} \geq 100$), as is the case here, paired echoes are strongly delayed with regard to the mainlobe [35]. Since we are interested in detecting close reverberation echoes, the sidelobes from paired echoes are not of concern and we shall only deal with sidelobes from steep band edges.

Edges in the amplitude spectrum of the pulse compression waveform $p(t)$ should, hence, be smoothed in order to achieve lower sidelobes. However, at the same time, this inevitably decreases the -6-dB bandwidth of the signal and, consequently, reduces axial resolution. Therefore, a tradeoff between smooth band edges, i.e., SLL, and axial resolution is necessary. This problem is common to, e.g., antenna shading, finite impulse response filter design, and for the implementation of the short Fourier transform [36]–[38].

In practice, smoothing of band edges can be achieved in two ways. The first method is to apply a filter $w(f)$ to the spectrum $P(f) \bullet\!\!-\!\!\circ p(t)$ that smoothly tapers the band edges. For chirps, a second approach is to appropriately modify the time domain matched filter by multiplying with a time limited and real function $w(t)$, called a "window." This is equivalent to a convolution in frequency domain, which inherently is a smoothing operation. Many window functions $w(t)$ have been designed whose Fourier transform $W(f)$ exhibits desired properties, e.g., low sidelobes and narrow main peaks. Let us note that this statement can be reversed due to the symmetry of the Fourier transform. Because if $w(t)$ is even, as is usual for window functions, and $w(t) \circ\!\!-\!\!\bullet W(f)$, then $w(f) \bullet\!\!-\!\!\circ W(t)$. Hence, such a filter $w(f)$ exhibits a narrow main peak and low sidelobes in time domain. An extensive review on different window functions is given by Harris [37]. The Dolph–Chebyshev window is an optimal window, exhibiting the narrowest mainlobe for given SLL [35], [37], [38]. It is, therefore, appropriate to keep good axial resolution while reducing the SLL. For this reason, it will be used in this contribution.

Let us look at sidelobe reduction for the Wiener filter, which we will perform by frequency domain filtering. If we desire to smooth the resulting band edges, we can simply apply a filter with frequency response $w(f) = w((f - f_c)a)$, consisting of a window function shifted and stretched to overlap exactly with the signal band. The Wiener filter behaves like an inverse filter on the signal band. If we idealize and assume that $|P(f)| = 1$ and its phase is zero, then the corresponding time domain signal envelope will be $W(t/a)$ except for a constant factor. Obviously, this time domain response inherently exhibits low sidelobes and a narrow mainlobe due to the design of the window. The pulse compression filter based on the Wiener filter with smoothing of band edges to reduced sidelobes is given by

$$K_{ww}(f) := \frac{w(f)G^*(f)}{G^*(f)G(f) + 1/\mathrm{SNR}_0}. \tag{39}$$
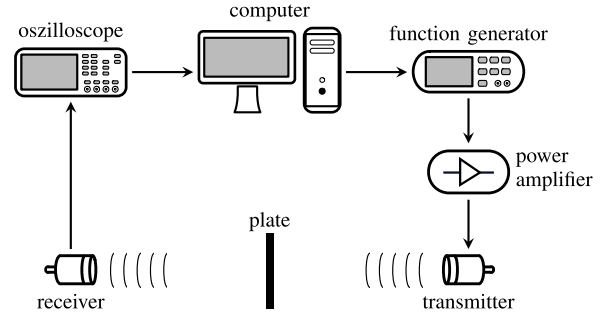
Fig. 10. Sketch of the measurement setup used to simultaneously determine a plate's thickness and the speed of sound.

Because $w(f)$ tapers at the band edges, (39) is basically a band limited inverse filter. We shall still use the Wiener filter notation for the sake of generality. The difference between the two will be marginal if the SNR_0 estimate is high enough.

To reduce the sidelobes of the matched filter, the same principle could be applied. Usually, however, windowing of the form

$$k_{mm}(t) := s^*(-t)w(t) \tag{40}$$

is applied instead. The resulting pulse compression filter is commonly called a *mismatched filter*. The amplitude spectrum of a chirp signal with high time-bandwidth product has approximately the shape of the chirp envelope [35]. This is a result of the fact that the instantaneous frequency of a chirp increases linearly with time. Therefore, a chirp with an envelope $w(t)$ features an approximately w-shaped amplitude spectrum. Thus, due to the properties of the chirp, this procedure offers similar results compared to applying the filter $w(f)$ as we did for the Wiener filter. Instead of applying the window function on the matched filter $k_m(t)$ to obtain a mismatched filter, it might be applied on the excitation signal $s(t)$ before transmit. Alternatively, it could be applied on both the excitation signal and the compression filter, which will result in stronger SLL reduction.

The SNR of a mismatched filter is about 1 dB lower than for a matched filter [19]. The reason for this small reduction in SNR is that the phase spectrum is still matched to the transmission signal, only the amplitude spectrum is mismatched, because the window function is purely real. Phase mismatching for SLL reduction could also be performed but is less robust [19]. In the next section, measurements with the presented excitation signal and pulse compression filters shall be performed and the results will be compared.

VI. MEASUREMENTS

A. Setup

A sketch of the full measurement setup is shown in Fig. 10. MATLAB (The MathWorks, Inc., Natick, MA, USA) is used to synthesize the transmission signal and to program the function generator (33500B, Agilent Technologies, Inc., Santa Clara, CA, USA). The latter excites the sending transducer through a power amplifier (3100LA, ENI Inc., Rochester, NY, USA) with 35-dB amplification, resulting in a peak excitation signal amplitude of 50 V. After transmitting through the
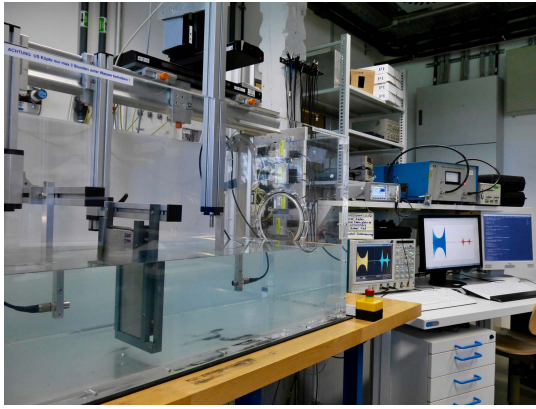
Fig. 11. Laboratory setup corresponding to Fig. 10.

Fig. 12. Measured axial PSFs of selected pulse compression techniques.

plate immersed in water, the acoustic signal is received by a transducer of the same type. An oscilloscope (DPO 7104C, Tektronix, Inc., Beaverton, OR, USA) samples the received signal at 200 MHz, averages over 50 recorded waveforms, and feeds the result back to the computer for further processing. In addition, the receiving transducer is mounted onto a linear traversing unit (M-531.DGX, Physik Instrumente GmbH & Co.KG, Karlsruhe, Germany), which is only utilized for the reference measurement.

The 1.27-cm planar ultrasonic transducers (V306, Olympus Corporation, Shinjuku, Tokyo, Japan) have a nominal center frequency of $f_c = 2.25$ MHz and a fractional bandwidth of $B = 61.45\%$ of the center frequency. Fig. 11 depicts the described laboratory setup.

We conducted the ultrasonic measurement in water to achieve better coupling into the plate, which is fully fixed. The transducers are guaranteed to transmit and receive perpendicular to the plate's surface by means of the suspension mechanisms.

B. Reference Measurement

With a view to simultaneously measuring the thickness and the speed of sound of the plate, it is necessary to know the speed of sound c_w in the surrounding medium, in our case water, and the geometric distance L between transmitter and receiver. We determine these two constants by means of a reference measurement without plate. This needs to be done only once before starting the actual measurements and also allows compensation of parameter variations, e.g., variations of c_w due to temperature changes.

The distance between the transducers can be varied with the traversing unit. After measuring the TOF at two different locations with well-known offset, the speed of sound in water and the distance between the transducers can be calculated. The TOFs are determined by the same pulse compression methods that will be used for measuring the plates.

C. Point Spread Function

The point spread function (PSF) in axial direction equals the waveform obtained after signal processing when only a directly transmitted signal without echoes is received,
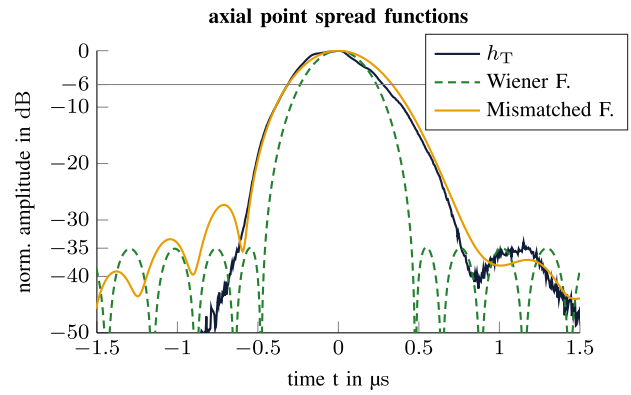
i.e., when no plate is located between the transducers. This corresponds to the compression output of an infinitely thin plate, i.e., the plate reduces to a point. Since in this case the compression output is not distorted by echoes, the width of the mainlobe determines the achievable axial resolution. Furthermore, the SLL is given by the height of the lobes. Hence, the PSF is useful to characterize the measurement system performance.

The measured PSFs for three different setups are displayed in Fig. 12. The first one shows the magnitude of the systems impulse response envelope $|\mathcal{H}\{h_T(t)\}|$, which is the PSF when the excitation signal is a short pulse like in traditional pulse-echo operation. The other two PSFs were both obtained using the conditioned excitation signal of Section IV-E, but each one uses a different pulse compression filter. One uses a Wiener filter with SLL reduction as described in (39), and the other one exploits a mismatched filter as in (40). In both cases, the filter $w(f)$ and the window $w(t)$ for SLL reduction are based on a Dolph–Chebyshev window targeting -35-dB SLL.

Fig. 12 demonstrates, as expected, that pulse compression of the interrogation signal with the smoothed Wiener filter achieves a better axial resolution than the traditionally employed short pulse response h_T. At the same time, smoothing with $w(f)$ ensures an acceptably low SLL. It should additionally be noted that the compression waveform of the Wiener filter is symmetric because the filter is designed on the basis of the expected interrogation signal, unlike the mismatched filter, which is designed on the basis of the chirp.

The mismatched filter $s(-t)w(t)$ exhibits a similar axial resolution compared to pulse-echo operation. Its SLL is considerably lower compared to the matched filter $s_c(-t)$ or the filter matched to $s(t)$ with rectangular window, i.e., $s(-t)$ (see Table I). Nonetheless, the SLL is higher than the targeted -35 dB because the conditioned signal is being compressed.

For matched or mismatched filtering, the conditioned excitation signal will naturally exhibit a higher SLL compared to the unconditioned one. This is evident due to the opposite behavior of the conditioning filter and the filter $w(f)$ for SLL reduction. While the conditioning filter tends to enhance the band edges, $w(f)$ is designed to smoothen them to achieve less steep edges.

TABLE I
COMPARISON OF AXIAL RESOLUTION AND SLL OF SELECTED
EXCITATION SIGNALS AND COMPRESSION FILTERS ($\delta_p = 0.59 \ \mu$s)

excitation signal	filter	$\frac{\Delta t}{\delta_p}$/1	SLL/dB
pulse	–	1.000	-33.9
chirp s	matched: $s(-t)$	1.060	-28.0
	mismatched: $s(-t)\mathrm{w}(t)$	1.323	-34.1
	smoothed Wiener: $K_{\mathrm{ww}}(f)$	0.802	-34.8
cond. chirp s_{c}	matched: $s_{\mathrm{c}}(-t)$	0.664	-7.5
	mismatched: $s_{\mathrm{c}}(-t)\mathrm{w}(t)$	0.859	-14.5
	mismatched: $s(-t)$	0.833	-14.5
	mismatched: $s(-t)\mathrm{w}(t)$	1.094	-27.3
	mismatched: $g_{\mathrm{c}}(-t)$	0.952	-29.4
	mismatched: $g_{\mathrm{c}}(-t)\mathrm{w}(t)$	0.986	-30.6
	smoothed Wiener: $K_{\mathrm{ww}}(f)$	0.801	-34.8

Table I shows the axial resolution and the SLL achieved with different combinations of excitation signal and pulse compression filters. The axial resolution Δt has been normalized to the axial resolution $\delta_p = 0.59 \ \mu$s achieved with a short pulse as excitation signal. As the table reveals, excitation signal conditioning does indeed substantially improve axial resolution for matched or mismatched filtering. The improved axial resolution is achieved at the expense of an increased SLL. As expected, a matched filter with conditioned excitation signal provides very good axial resolution. However, SLL performance is unacceptably low. The Dolph–Chebyshev window is capable of providing good axial resolution at given desired SLL. Matching the filter to $s_c(t)$ will yield good axial resolution, while matching it to $s(t)$ provides better SLL. It is interesting to note that the Wiener filter performance is basically independent of the excitation signal. This is because it acts as an inverse filter in the frequency band which falls within the smoothing filter $w(f)$ that is applied.

Due to the combination of axial resolution performance and SLL, we selected the Wiener filter with a -35-dB Dolph–Chebyshev function as smoothing filter. Measurements showed that an SNR estimate of $\mathrm{SNR}_0 = 1000$ provides good results. Due to the bandpass filter $w(f)$ applied for SLL reduction, this compression filter is not very sensitive to the choice of SNR_0. In addition, we use a filter mismatched to $s(t)$ with a -35-dB Dolph–Chebyshev window function applied in time domain to conduct the measurements.

D. Compression Output of Plate's Response

Fig. 13 shows the compression output $\iota(t) = |\mathcal{H}\{p(t)\}|$ for three steel plates of different thicknesses. Pulse compression was performed with the selected compression filters. For the thinnest plate, the mismatched filter response does not exhibit any peaks since they melt together. This means that the axial resolution is not sufficient to measure such a thin plate. On the contrary, the tapered Wiener filter is able to provide the necessary resolution as the peaks can clearly be identified.

E. Measurement Results

In order to actually measure the thickness of plates and the speed of sound within them, we employed the conditioned
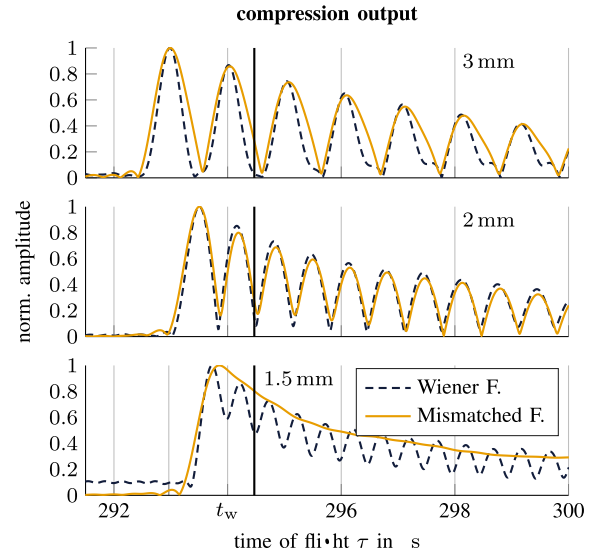
Fig. 13.   Compression output for different plates with the selected Wiener filter and mismatched filter (-35-dB Dolph–Chebyshev). Plate thickness is given in millimeter.
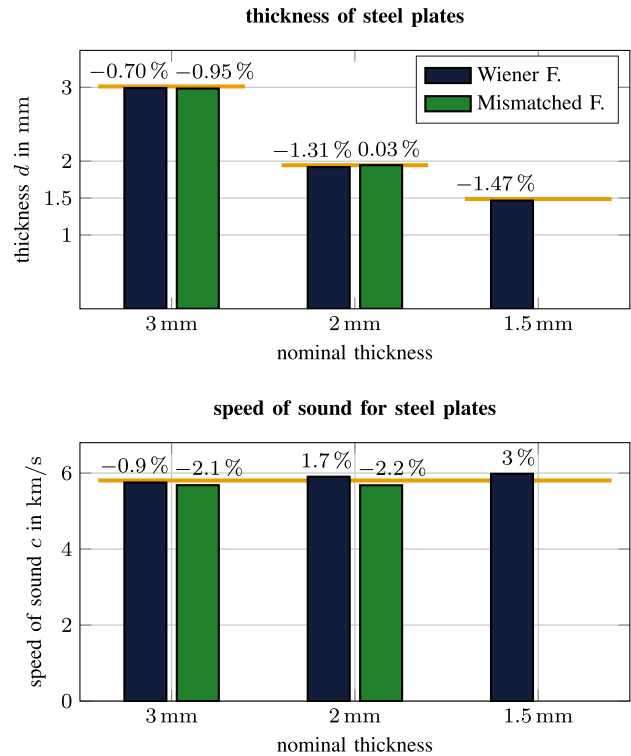
Fig. 14.   Measurement results for steel plates of different thicknesses.

excitation signal $\bar{s}_c(t)$ for interrogation. Again, both selected filters were used for pulse compression. The peaks in the compression output and their temporal locations (see Fig. 13) were found algorithmically. The compression output was normalized to its maximum. Peaks were required to be greater than 0.15 to avoid detection of sidelobes. The TOF differences between adjacent peaks were calculated and their mean was considered the best estimate for the echo delay T. Together
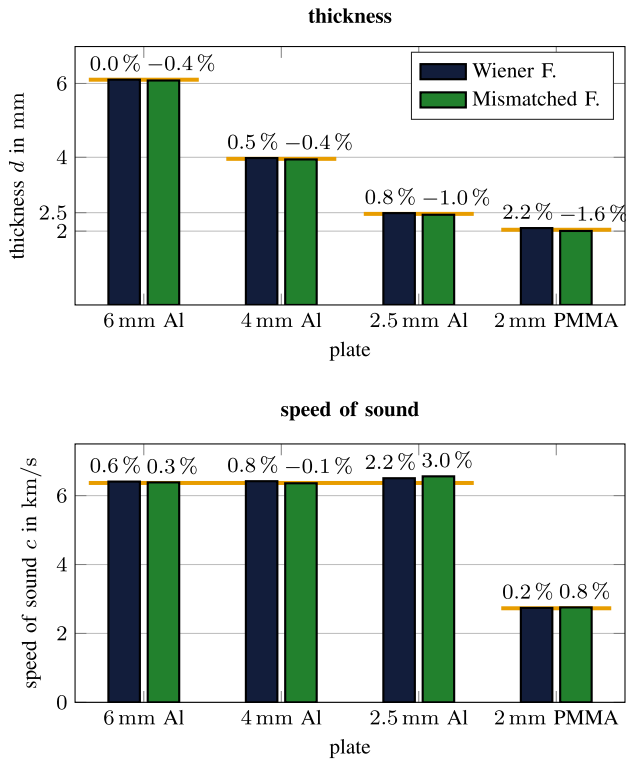
Fig. 15.   Measurement results for aluminum and PMMA plates.

with the arrival time t_0 of the directly transmitted signal, which corresponds to the location of the highest peak, and the TOF in water t_w known from the reference measurement, the thickness d and the speed of sound c can be calculated by (1) and (2). Therefore, the entire measurement is fully automated.

Different plates of steel (EN 1.4541 from REMAG AG), aluminum (EN AW-5754 from Hans-Erich Gemmel & Co. GmbH) as well as polymethylmethacrylate (PMMA, acrylic glass from König GmbH) were characterized. The results are shown in Figs. 14 and 15. A micrometer screw gauge (Mitutoyo 102-217) was used to measure the thickness of the plate at six different positions. The mean value serves as the plate's reference thickness. The micrometer screw's accuracy is about 0.02 mm. A standard TOF measurement with a contact longitudinal transducer was performed to determine the reference value for the speed of sound. For this reference measurement, a transducer with 10-MHz center frequency and 112% fractional bandwidth was used (V112, Olympus Corporation, Shinjuku, Tokyo, Japan). All reference values are displayed as horizontal lines in the plots. The relative deviation of the proposed ultrasonic measurement from the reference is given in percent above the bars. This deviation stems from uncertainty in the presented ultrasonic measurement technique as well as the reference measurements. The former is based solely on relative TOF measurements as given in (1) and (2). The precision herefor is mainly restricted by the sampling period of 5 ns, which for the worst case of a 1.5-mm-thick steel plate results in 0.8% maximum relative error in the calculated thickness and 1.2% for the speed of

sound. The positioning uncertainty of the linear traversing unit used to determine c_w and L (or t_w) equals 0.2 μm and is therefore negligible. Material and geometric inhomogeneity introduce further uncertainty. The mismatched filter does not provide sufficient axial resolution to measure the 1.5-mm-thick plate and the results are, hence, missing in the graph.

For all samples, the measurement results exhibit very good agreement with the references. The relative error for the measured thickness stays below 2.2%. The poorest result was achieved with the PMMA plate, which can probably be ascribed to material inhomogeneity in thickness direction due to mechanical processing at the plate's faces [39]. It is remarkable that the plate thickness could be measured down to 60% of the wavelength. For the speed of sound the relative error is below 3% and, therefore, also coincides well with the references.

VII. CONCLUSION

The thickness of a homogeneous plate and the speed of sound of its material can be measured simultaneously. In transmission mode, the distance between the transmitting and receiving transducers, as well as the speed of sound of the surrounding medium, need to be known in advance. These values were determined by a reference measurement. By means of TOF measurement of reverberation echoes, the sought quantities can be calculated.

A theoretical transmission model, both in time and frequency domain, were given. The needed TOF information can either be extracted out of the impulse response or the transfer function. We also found that the axial resolution of the measurement system determines the smallest ratio of thickness to the speed of sound that can be measured. Therefore, to measure thin plates of unknown material, good axial resolution is required.

The excitation signal that drives the ultrasonic transducer should comply with two main requirements. First, sufficiently high bandwidth is needed to provide the necessary axial resolution. Second, high energy accounts for good SNR. This is achieved best using a signal with high time-bandwidth product $\bar{D}\bar{B}$, the so-called coded signals. A LFM signal, also called linear chirp, with $\bar{D}\bar{B} \approx 430$, was used in this contribution.

Signal conditioning can be performed on the excitation signal in order to enhance the bandwidth of the interrogation signal. This consists in boosting the spectral components that are not transmitted efficiently by the transducer. We presented a new approach for the conditioning filter and for the ideal transducer model. This approach provides the advantage that it avoids phase distortion of the excitation signal and the ideal transducer is easier to design. Another advantage is that the pulse compression filter can be designed on the basis of the nonconditioned chirp instead of the conditioned chirp being transmitted. As the results demonstrate, signal conditioning can provide considerably improved axial resolution after pulse compression. However, it is not necessary when using a Wiener filter or band-limited inverse filter. These filters provide

best axial resolution essentially independent of the excitation signal.

A Wiener filter with smoothing and a mismatched filter were used to perform measurements and the results were compared. The measured plate thickness as well as the speed of sound both showed very good agreement with the reference values. The Wiener filter is capable of measuring slightly thinner plates than the mismatched filter with conditioned excitation signal.

The proposed signal conditioning for bandwidth enhancement can be applied to any class of excitation signals. Future work should analyze the achievable performance improvements of phase coded signals, such as Barker codes. Moreover, the time delay between reverberation echoes is constant. This is *a priori* knowledge, which is not exploited by the presented ultrasonic imaging approach for measuring plates. This could be accomplished by fitting an appropriate parametric signal model to the measured data.

REFERENCES

[1] S. J. Rupitsch, D. Glaser, and R. Lerch, "Simultaneous determination of speed of sound and sample thickness utilizing coded excitation," in *Proc. IEEE Int. Ultrason. Symp. (IUS)*, Oct. 2012, pp. 711–714.

[2] D. K. Hsu and M. S. Hughes, "Simultaneous ultrasonic velocity and sample thickness measurement and application in composites," *J. Acoust. Soc. Amer.*, vol. 92, no. 2, pp. 669–675, Aug. 1992.

[3] X. Bai, Z. Sun, J. Chen, and B.-F. Ju, "A novel technique for the measurement of the acoustic properties of a thin linear-viscoelastic layer using a planar ultrasonic transducer," *Meas. Sci. Technol.*, vol. 24, no. 12, p. 125602, 2013.

[4] V. K. Kinra and V. R. Iyer, "Ultrasonic measurement of the thickness, phase velocity, density or attenuation of a thin-viscoelastic plate. Part I: The forward problem," *Ultrasonic*, vol. 33, no. 2, pp. 95–109, 1995.

[5] S. Harput, T. Evans, N. Bubb, and S. Freear, "Diagnostic ultrasound tooth imaging using fractional Fourier transform," *IEEE Trans. Ultrason., Ferroelect., Freq. Control*, vol. 58, no. 10, pp. 2096–2106, Oct. 2011.

[6] V. K. Kinra and V. R. Iyer, "Ultrasonic measurement of the thickness, phase velocity, density or attenuation of a thin-viscoelastic plate. Part II: The inverse problem," *Ultrasonic*, vol. 33, no. 2, pp. 111–122, 1995.

[7] V. K. Kinra and V. Dayal, "A new technique for ultrasonic-nondestructive evaluation of thin specimens," *Experim. Mech.*, vol. 28, no. 3, pp. 288–297, Sep. 1988.

[8] C. Zhu and V. K. Kinra, "A new technique for time-domain ultrasonic NDE of thin plates," *J. Nondestruct. Eval.*, vol. 12, no. 2, pp. 121–131, Jun. 1993.

[9] S. J. Rupitsch, J. Ilg, A. Sutor, R. Lerch, and M. Döllinger, "Simulation based estimation of dynamic mechanical properties for viscoelastic materials used for vocal fold models," *J. Sound Vibrat.*, vol. 330, nos. 18–19, pp. 4447–4459, Sep. 2011.

[10] J. Ilg, S. J. Rupitsch, A. Sutor, and R. Lerch, "Determination of dynamic material properties of silicone rubber using one-point measurements and finite element simulations," *IEEE Trans. Instrum. Meas.*, vol. 61, no. 11, pp. 3031–3038, Nov. 2012.

[11] C. Graciet and B. Hosten, "Simultaneous measurement of speed, attenuation, thickness and density with reflected ultrasonic waves in plates," in *Proc. IEEE Ultrason. Symp*, vol. 2. Oct. 1994, pp. 1219–1222.

[12] D. T. Blackstock, *Fundamentals of Physical Acoustics*. Hoboken, NJ, USA: Wiley, Apr. 2000.

[13] R. Lerch, G. M. Sessler, and D. Wolf, *Technische Akustik: Grundlagen und Anwendungen*, 1st ed. Berlin, Germany: Springer, Sep. 2009.

[14] K. Altenburg and S. Kästner, "Wellenausbreitung in geschichteten Medien bei senkrechtem Einfall und die Anwendung auf Leitungstheorie, elektrische Wellen, Optik, Akustik, Wellenmechanik sowie mechanische und elektrische Vierpolketten," *Ann. Phys.*, vol. 448, nos. 1–5, pp. 1–43, Jan. 1953.

[15] J. L. Rose, *Ultrasonic Waves in Solid Media*. Cambridge, U.K.: Cambridge Univ. Press, Sep. 2004.

[16] I. N. Bronstein, K. A. Semendjajew, G. Musiol, and H. Mühlig, *Taschenbuch der Mathematik*. 7th ed. Frankfurt, Germany: Harri Deutsch, Aug. 2000.

[17] J. Ohm and H. D. Lüke, *Signalübertragung: Grundlagen der Digitalen und Analogen Nachrichtenübertragungssysteme*, 12th ed. Berlin, Germany: Springer-Verlag, Feb. 2015.

[18] C. E. Cook, "Pulse compression-key to more efficient radar transmission," *Proc. IRE*, vol. 48, no. 3, pp. 310–316, Mar. 1960.

[19] T. Misaridis and J. A. Jensen, "Use of modulated excitation signals in medical ultrasound. Part I: Basic concepts and expected benefits," *IEEE Trans. Ultrason., Ferroelect., Freq. Control*, vol. 52, no. 2, pp. 177–191, Feb. 2005.

[20] S. Venkatraman and N. A. H. K. Rao, "Combining pulse compression and adaptive drive signal design to inverse filter the transducer system response and improve resolution in medical ultrasound," *Med. Biol. Eng. Comput.*, vol. 34, no. 4, pp. 318–320, Jul. 1996.

[21] Z. Zhou *et al.*, "Application of wavelet filtering and Barker-coded pulse compression hybrid method to air-coupled ultrasonic testing," *Nondestruct. Test. Eval.*, vol. 29, no. 4, pp. 297–314, 2014.

[22] L. Cohen, "Time-frequency distributions—A review," *Proc. IEEE*, vol. 77, no. 7, pp. 941–981, Jul. 1989.

[23] A. W. Rihaczek, "Radar signal design for target resolution," *Proc. IEEE*, vol. 53, no. 2, pp. 116–128, Feb. 1965.

[24] R. Y. Chiao and X. Hao, "Coded excitation for diagnostic ultrasound: A system developer's perspective," *IEEE Trans. Ultrason., Ferroelect., Freq. Control*, vol. 52, no. 2, pp. 160–170, Feb. 2005.

[25] R. E. Blahut, W. Miller, and C. H. Wilcox, *Radar and Sonar: Part I*. New York, NY, USA: Springer-Verlag, May 1991.

[26] R. C. Gonzalez and R. E. Woods, *Digital Image Processing*, 3rd ed. Upper Saddle River, NJ, USA: Addison-Wesley, Jul. 2008.

[27] H. Hasegawa, S. Kageyama, and H. Kanai, "Improvement of axial spatial resolution of ultrasound image using Wiener filter for measurement of intima-media thickness of carotid artery," in *Proc. IEEE Int. Ultrason. Symp. (IUS)*, Jul. 2013, pp. 1232–1235.

[28] R. Raman and N. Rao, "Pre-enhancement of chirp signal for inverse filtering in medical ultrasound," in *Proc. 16th Annu. Int. Conf. IEEE Eng. Med. Biol. Soc. Eng. Adv., New Opportunities Biomed. Eng.*, vol. 1. Nov. 1994, pp. 676–677.

[29] M. L. Oelze, "Bandwidth and resolution enhancement through pulse compression," *IEEE Trans. Ultrason., Ferroelect., Freq. Control*, vol. 54, no. 4, pp. 768–781, Apr. 2007.

[30] M. L. Oelze, "1K-2 improved axial resolution using pre-enhanced chirps and pulse compression," in *Proc. IEEE Int. Ultrason. Symp. (IUS)*, Oct. 2006, pp. 1083–1086.

[31] M. Pollakowski, H. Ermert, L. von Bernus, and T. Schmeidl, "The optimum bandwidth of chirp signals in ultrasonic applications," *Ultrasonic*, vol. 31, no. 6, pp. 417–420, Nov. 1993.

[32] D. M. J. Cowell and S. Freear, "Separation of overlapping linear frequency modulated (LFM) signals using the fractional Fourier transform," *IEEE Trans. Ultrason., Ferroelect., Freq. Control*, vol. 57, no. 10, pp. 2324–2333, Oct. 2010.

[33] F. Zhang, R. Tao, and Y. Wang, "Analysis and processing for chirp pulse with matched FRFT," in *Proc. 2nd Int. Conf. Instrum. Meas. Comput. Commun. Control (IMCCC)*, Dec. 2012, pp. 5–9.

[34] A. Akhavan, A. Mahloojifar, and S. Hashemi-Berenjabad, "Axial resolution and robustness improvement in coded excitation ultrasound images using fractional Fourier transform," in *Proc. Develop. E-Syst. Eng. (DeSE)*, Dec. 2011, pp. 68–73.

[35] T. Misaridis and J. A. Jensen, "Use of modulated excitation signals in medical ultrasound. Part II: Design and performance for medical imaging applications," *IEEE Trans. Ultrason., Ferroelect., Freq. Control*, vol. 52, no. 2, pp. 192–207, Feb. 2005.

[36] A. V. Oppenheim and R. W. Schafer, *Discrete-Time Signal Processing*, 3rd ed. Upper Saddle River, NJ, USA: Addison-Wesley, Aug. 2009.

[37] F. J. Harris, "On the use of windows for harmonic analysis with the discrete Fourier transform," *Proc. IEEE*, vol. 66, no. 1, pp. 51–83, Jan. 1978.

[38] P. Lynch, "The Dolph–Chebyshev window: A simple optimal filter," *Monthly Weather Rev.*, vol. 125, no. 4, pp. 655–660, Apr. 1997.

[39] L. Chen, S. J. Rupitsch, J. Grabinger, and R. Lerch, "Quantitative reconstruction of ultrasound fields in optically transparent isotropic solids," *IEEE Trans. Ultrason., Ferroelect., Freq. Control*, vol. 61, no. 4, pp. 685–695, Apr. 2014.

Daniel A. Kiefer was born in Tumbaco-Quito, Ecuador, in 1989. He received the B.Sc. and M.Sc. degrees in mechatronics from the Friedrich-Alexander-University of Erlangen–Nuremberg, Erlangen, Germany, in 2013 and 2016, respectively, where he is currently pursuing the Ph.D. degree in ultrasonic measurement with the Chair of Sensor Technology.

His research interests include ultrasonic imaging and measurement, elastodynamics, electromechanical transducers, as well as energy harvesting.

Michael Fink (S'15) was born in Regensburg, Germany, in 1984. He received the M.Sc. degree in mechatronics from the Friedrich-Alexander-University of Erlangen–Nuremberg, Erlangen, Germany, in 2014, where he is currently pursuing the Ph.D. degree with the Chair of Sensor Technology.

His current research interests include medical ultrasound imaging and signal processing.

Stefan J. Rupitsch (S'07–M'09) was born in Kitzbuehel, Austria, in 1978. He received the Diploma and Ph.D. degrees in mechatronics from Johannes Kepler University, Linz, Austria, in 2004 and 2008, respectively.

He was a Junior Researcher with the Linz Center of Mechatronics, Linz, in 2004. From 2005 to 2008, he was with the Institute for Measurement Technology, Johannes Kepler University. He is currently a Post-Doctoral Researcher with the Friedrich-Alexander-University of Erlangen–Nuremberg (Chair of Sensor Technology), Erlangen, Germany. He has authored more than 100 papers. His current research interests include electromechanical transducers, simulation-based material characterization, acoustic microscopy, digital signal and image processing, as well as noncontacting measurements.

Dr. Rupitsch was a recipient of the Austrian Society of Measurement and Automation Technology Award for his Ph.D. thesis in 2009 and the Outstanding Paper Award of the Information Technology Society in 2016. He is an Associate Editor of the IEEE Sensors Journal.